
Group Knowledge Transfer: Collaborative Training of Large CNNs on the Edge

Chaoyang He Salman Avestimehr Murali Annavaram

University of Southern California

Los Angeles, CA 90007

chaoyang.he@usc.edu annavara@usc.edu avestime@usc.edu

Abstract

Scaling up the convolutional neural network (CNN) size (e.g., width, depth, etc.) is known to effectively improve model accuracy. However, the large model size impedes *training* on resource-constrained edge devices. For instance, federated learning (FL) on edge devices cannot tackle large CNN training demands, even though there is a strong practical need for FL due to its privacy and confidentiality properties. To address the resource-constrained reality, we reformulate FL as a group knowledge transfer (GKT) training algorithm. GKT designs a variant of the alternating minimization approach to train small CNNs on edge nodes and periodically transfer their knowledge by knowledge distillation to a large server-side CNN. GKT consolidates several advantages in a single framework: reduced demand for edge computation, lower communication cost for large CNNs, and asynchronous training, all while maintaining model accuracy comparable to FL. To simplify the edge training, we also develop a distributed training system based on our GKT. We train CNNs designed based on ResNet-56 and ResNet-110 using three distinct datasets (CIFAR-10, CIFAR-100, and CINIC-10) and their non-IID variants. Our results show that GKT can obtain comparable or even slightly higher accuracy. More importantly, GKT makes edge training affordable. Compared to the edge training using FedAvg, GKT demands 9 to 17 times less computational power (FLOPs) on edge devices and requires 54 to 105 times fewer parameters in the edge CNN.

1 Introduction

The size of convolutional neural networks (CNN) matters. As seen in both manually designed neural architectures (ResNet [1]) and automated architectures discovered by neural architecture search (DARTS [2], MiLeNAS [3], EfficientNets [4]), scaling up CNN size (e.g., width, depth, etc.) is known to be an effective approach for improving model accuracy. Unfortunately, training large CNNs is challenging for resource-constrained edge devices (e.g., smartphones, IoT devices, and edge servers). However, the demand for edge-based training is increasing as evinced by a recent upsurge of research interest in Federated Learning (FL) [5]. FL is a distributed learning paradigm that can collaboratively train a common model for many edge devices without centralizing any device's dataset [6, 7, 8]. FL can boost model accuracy through collaborative training on private data in situations when a single organization or user does not have sufficient or relevant data. Consequently, many FL services have been deployed (e.g., Google has improved the accuracy of item ranking and language models on Android smartphones by using FL [9]). FL is also a promising solution when data centralization is undesirable or infeasible due to privacy and regulatory constraints [5]. However, one significant impediment in edge training is the gap between the computational demand of large CNNs and the meager computational power on edge devices. FL approaches (FedAvg [6], FedProx [10], and FedMA [8]) can reduce communication frequency by local SGD and model averaging [11],

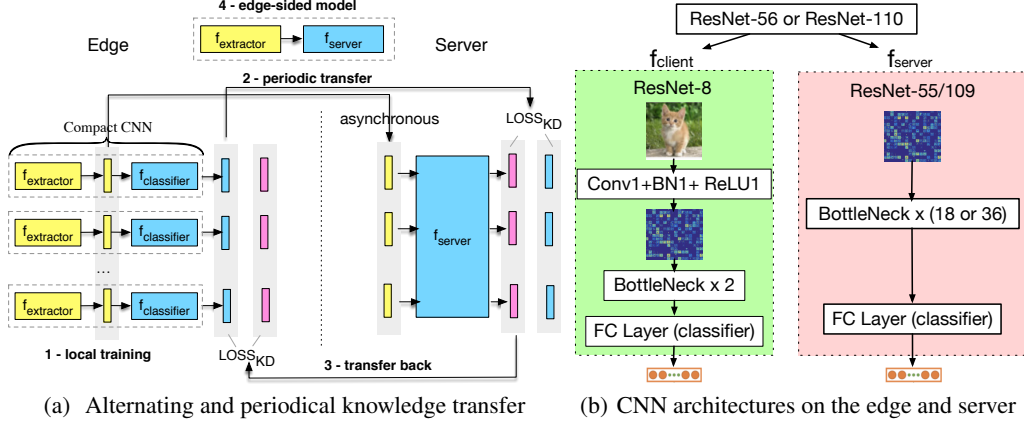


Figure 1: Reformulation of Federated Learning: Group Knowledge Transfer

but they only evaluate the convergence property on small CNNs, or assume the client has enough computational power and run large CNNs with the GPU accelerator, which is unrealistic in real-world system. To tackle the computational limitation of edges, model parallelism-based split learning (SL) [12, 13] partitions a large model and offloads the larger portion of the neural architecture to the cloud. Nevertheless, the obvious drawback of SL is that it has a severe straggler problem because of its highly frequent synchronization mechanism in which a single mini-batch iteration requires multiple rounds of communication between the server and edges.

In this paper, we propose Group Knowledge Transfer (GKT), an efficient collaborative training framework for resource-constrained edge devices. GKT aims to incorporate benefits from both FedAvg [6] and SL [12, 13] by training locally as in FL but also computing efficiently as in SL. GKT can transfer knowledge from many compact CNNs to a large CNN. The essence of GKT is that it reformulates FL as an alternating minimization (AM) approach [14, 15, 16, 17, 18, 19], which optimizes two random variables (the edge model and the server model) by alternatively fixing one and optimizing another. Under this reformulation, GKT further develops a new knowledge distillation (KD) paradigm, group knowledge transfer, to boost the performance of the server model. As shown in Fig. 1(a), the compact CNN contains a lightweight feature extractor and classifier inside and is thus efficiently trainable on edge devices using their private data (1 - local training). After local training, all the edge nodes agree to generate *exactly* the same tensor dimensions as an output from the feature extractor. The larger server model is trained by taking features extracted from the edge-side model and also computing a KD-based loss function using the ground truth and soft label (the probabilistic prediction in KD [20, 21, 22, 23]) predicted from the edge-side model (2 - periodic transfer). To boost the edge model’s performance, the server sends its predicted soft labels to the edge, then the edge also trains its local dataset with a KD-based loss function using server-side soft labels (3 - transfer back). Thus, the server’s performance is essentially boosted by knowledge transferred from the edge models and vice-versa. Once the training is complete after many rounds of communication, each edge’s final model is a combination of its local feature extractor and shared server model (4 - edge-sided model). The primary trade-off is that GKT shifts the computing burden from edge devices to server-side since the large CNN must be trained on the GPU-equipped server.

GKT unifies multiple advantages into a single framework: 1. GKT is computationally and memory-efficient, similar to SL; 2. GKT can train in a local SGD manner like FL to reduce the communication frequency; 3. Exchanging hidden features as in SL, as opposed to exchanging the entire model as in FL, reduces the communication cost. 4. GKT naturally supports asynchronous training, which circumvents the severe synchronization issue in SL. As shown in Fig. 1(a), the server model can immediately start training when it receives inputs from any client. We develop a distributed training system for GKT and comprehensively evaluate GKT using edge and server CNNs designed based on ResNet [1] (as shown in Fig. 1(b)). We train on three datasets with varying training difficulties (CIFAR-10 [24], CIFAR-100 [24], and CINIC-10 [25]) and their non-IID (non identical and independent distribution) variants. As for the model accuracy, our results on both IID and non-IID datasets show that GKT can obtain accuracy comparable to FedAvg [6]. More importantly, GKT makes edge training affordable. Compared to FedAvg, GKT demands 9 to 17 times less computational power (FLOPs) on edge devices and requires 54 to 105 times fewer parameters in the edge CNN. To understand GKT comprehensively, asynchronous training and ablation studies are also performed.

2 Related Works

Federated Learning. Existing FL methods such as FedAvg [6], FedProx [10], and FedMA [8] face significant hurdles in training large CNNs on resource-constrained devices. Recent works [26] [27] analyze the performance of FedAvg in large CNNs, but they rely on GPU training to complete the evaluations. Others [28, 29, 30, 31, 32, 33] optimize the communication cost without considering edge computational limitations. Model parallelism-based split learning [12, 13] attempts to break the computational constraint, but it requires frequent communication with the server. **Knowledge Distillation (KD).** We use KD [20] in a different way from existing works. Previous works only consider transferring knowledge from a large network to a smaller one [20, 21, 22, 23], or they transfer knowledge from a group, but each member in the group shares the same large model architecture or a large portion of the neural architecture with specific tail or head layers [34, 35, 36, 37, 38, 39]. Moreover, all teachers and students in distillation share the same dataset [38, 40, 41, 42], while in our setting each member (client) can only access its own independent dataset. Previous methods use centralized training, but we utilize an alternating training method. **Efficient On-device Deep Learning.** Our work also relates to efficient deep learning on edge devices, such as model compression [43, 44, 45], manually designed architectures (MobileNets [46], ShuffleNets [47], SqueezeNets [48]), or even efficient neural architecture search (EfficientNets [4], FBNet [49]). However, all of these techniques are tailored for the inference phase rather than the training phase.

3 Group Knowledge Transfer

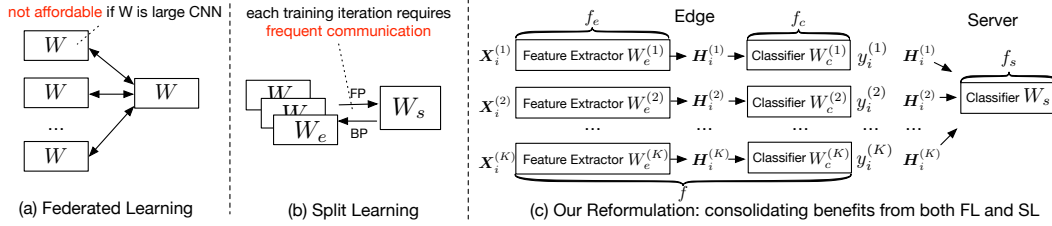


Figure 2: Reformulation of FL: An Alternating Minimization Perspective

3.1 Preliminary

We aim to collaboratively train large convolutional neural networks (e.g., ResNet) on many resource-constrained devices that are not equipped with GPU accelerators without centralizing each device’s dataset to the server side. We specifically consider supervised learning with C categories in the entire dataset \mathcal{D} . We assume that there are K clients (edge devices) in the network. The k th node has its own dataset $\mathcal{D}^k := \left\{ \left(\mathbf{X}_i^k, y_i \right) \right\}_{i=1}^{N^{(k)}}$, where \mathbf{X}_i is the i th training sample, y_i is the corresponding label of \mathbf{X}_i , $y_i \in \{1, 2, \dots, C\}$ (a multi-classification learning task), and $N^{(k)}$ is the sample number in dataset \mathcal{D}^k . $\mathcal{D} = \{\mathcal{D}_1, \mathcal{D}_2, \dots, \mathcal{D}_K\}$, $N = \sum_{k=1}^K N^{(k)}$.

FedAvg [6] formulates the objective function of DNN-based federated learning as:

$$\min_{\mathbf{W}} F(\mathbf{W}) \stackrel{\text{def}}{=} \min_{\mathbf{W}} \sum_{k=1}^K \frac{N^{(k)}}{N} \cdot f^{(k)}(\mathbf{W}), \text{ where } f^{(k)}(\mathbf{W}) = \frac{1}{N^{(k)}} \sum_{i=1}^{N^{(k)}} \ell(\mathbf{W}; \mathbf{X}_i, y_i) \quad (1)$$

where \mathbf{W} represents the network weight of a global CNN in each client. $f^{(k)}(\mathbf{W})$ is the k th client’s local objective function that measures the local empirical risk over the heterogeneous dataset \mathcal{D}^k . ℓ is the loss function of the global CNN model.

The objective function (1) is viewed as a distributed optimization problem and can also be solved using off-the-shelf algorithms (e.g., FedProx [10] and FedMA [8]). These methods utilize local SGD and model averaging [11] for communication-efficient training. However, as shown in Fig. 2(a), the main drawback of FL is that existing methods cannot address the resource-constrained nature of edge devices. Model parallelism-based split learning [12, 13], as shown in Fig. 2(b), attempts to break the computational constraint by splitting \mathbf{W} into two portions and offloading the larger portion into the server-side, but a single mini-batch iteration requires remote forward propagation

and backpropagation. For edge computing, such a highly frequent synchronization mechanism may lead to the severe straggler problem that significantly slows down the training process.

3.2 Reformulation

Non-convex Optimization. To solve the resource-constrained problem in existing FL, we reconsider another methodology to solve the FL optimization problem. As illustrated in Fig. 2(c), we divide the global CNN \mathbf{W} in Eq. (1) into two partitions: a small feature extractor model \mathbf{W}_e and a large-scale server-side model \mathbf{W}_s , and put them on the edge and the server, respectively. We also add a classifier \mathbf{W}_c for \mathbf{W}_e to create a small but fully trainable model on the edge. Consequently, we reformulate a single global model optimization into a non-convex optimization problem that requires us to solve the edge model and the server model simultaneously. Our reformulation is as follows:

$$\underset{\mathbf{W}_s}{\operatorname{argmin}} F_s(\mathbf{W}_s, \mathbf{W}_e^*) = \underset{\mathbf{W}_s}{\operatorname{argmin}} \sum_{k=1}^K \sum_{i=1}^{N^{(k)}} \ell_s \left(f_s(\mathbf{W}_s; \mathbf{H}_i^{(k)}), y_i^{(k)} \right) \quad (2)$$

$$\text{subject to: } \mathbf{H}_i^{(k)} = f_e^{(k)}(\mathbf{W}_e^{(k)}; \mathbf{X}_i^{(k)}) \quad (3)$$

$$\underset{(\mathbf{W}_e^{(k)}, \mathbf{W}_c^{(k)})}{\operatorname{argmin}} F_c(\mathbf{W}_e^{(k)}, \mathbf{W}_c^{(k)}) = \underset{(\mathbf{W}_e^{(k)}, \mathbf{W}_c^{(k)})}{\operatorname{argmin}} \sum_{i=1}^{N^{(k)}} \ell_c \left(f^{(k)}((\mathbf{W}_e^{(k)}, \mathbf{W}_c^{(k)}); \mathbf{X}_i^{(k)}), y_i^{(k)} \right) \quad (4)$$

$$= \underset{(\mathbf{W}_e^{(k)}, \mathbf{W}_c^{(k)})}{\operatorname{argmin}} \sum_{i=1}^{N^{(k)}} \ell_c \left(f_c^{(k)}(\mathbf{W}_c^{(k)}; \underbrace{f_e^{(k)}(\mathbf{W}_e^{(k)}; \mathbf{X}_i^{(k)})}_{\mathbf{H}_i^{(k)}}), y_i^{(k)} \right) \quad (5)$$

Where ℓ_s and ℓ_c are general loss functions for the server model and the edge model, respectively. f_s is the server model, and $f^{(k)}$ is the edge-side model which consists of feature extractor $f_e^{(k)}$ followed by a classifier $f_c^{(k)}$. \mathbf{W}_s , $\mathbf{W}_e^{(k)}$, $\mathbf{W}_c^{(k)}$ are the network weights of f_s , $f_e^{(k)}$, $f_c^{(k)}$, respectively. $\mathbf{H}^{(k)}$ is the feature map (a hidden vector or tensor) output by feature extractor $f_e^{(k)}$ (Eq. (3)). The k th client model $f^{(k)}$ is trained on its local dataset (Eq. (5)), while the server model f_s is trained using $\mathbf{H}^{(k)}$ as input features (Eq. (2)). The final trained model architecture for client k is stacked by the architecture of the feature extractor $f_e^{(k)}$ and the architecture of the server model f_s .

Advantages and Challenges. The core advantage of the above reformulation is that when we assume the model size of $f^{(k)}$ is multiple orders of magnitude smaller than that of f_s , the edge training is affordable. Moreover, as discussed in [12, 13], for large CNN training, the communication bandwidth for transferring $\mathbf{H}^{(k)}$ to the server is substantially less than communicating the whole model parameters as is done in traditional federated learning. Conversely, we also observe the difficulty of the reformulated optimization problem. First, each client is expected to adequately solve the inner optimization (Eq. (5)). Namely, each client must train its feature extractor $f_e^{(k)}$ well to accurately generate $\mathbf{H}^{(k)}$ for any given input image using Eq. (3). However, in the FL setting, the dataset on each edge device is small and thus may be inadequate in training a CNN-based feature extractor solely based on the local dataset. Second, the outer optimization Eq. (2) and inter optimization Eq. (5) are correlated. This correlation further makes the outer optimization difficult to converge if the individual client-side feature extractors are not trained adequately.

3.3 Group Knowledge Transfer (GKT)

Scaling Edge Dataset Limitations with Knowledge Transfer. Given the above challenges, we incorporate knowledge distillation loss into the optimization equations to circumvent the optimization difficulty. The intuition is that knowledge transferred from the the server model can boost the optimization on the edge (Eq. (5)). As such, we propose to transfer group knowledge from edge-side CNNs to the server CNN. To be more specific, in Eq. (2) and (5), we design ℓ_s and ℓ_c as follows.

$$\ell_s = \ell_{CE} + \sum_{k=1}^K \ell_{KD} \left(\mathbf{z}_s, \mathbf{z}_c^{(k)} \right) = \ell_{CE} + \sum_{k=1}^K D_{KL}(\mathbf{p}_k \| \mathbf{p}_s) \quad (6)$$

$$\ell_c^{(k)} = \ell_{CE} + \ell_{KD} \left(\mathbf{z}_s, \mathbf{z}_c^{(k)} \right) = \ell_{CE} + D_{KL}(\mathbf{p}_s \| \mathbf{p}_k) \quad (7)$$

ℓ_{CE} is the cross-entropy loss between the predicted values and the ground truth labels. D_{KL} is the Kullback Leibler (KL) Divergence function that serves as a term in the loss function ℓ_s and ℓ_c to transfer knowledge from a network to another. $p_k^i = \frac{\exp(z_c^{(k,i)}/T)}{\sum_{i=1}^C \exp(z_c^{(k,i)}/T)}$ and $p_s^i = \frac{\exp(z_s^i/T)}{\sum_{i=1}^C \exp(z_s^i/T)}$.

They are the probabilistic prediction of the client model $f^{(k)}$ and the server model f_s , respectively. They are calculated with the softmax of logits z . The logit z is the output of the last fully connected layer in a neural network, and T is the temperature hyperparameter of the softmax function.

Intuitively, the KL divergence loss attempts to bring the soft label and the ground truth close to each other. In doing so, the server model absorbs the knowledge gained from each of the edge models. Similarly, the edge models try to bring their predictions closer to the prediction of server model and thereby absorb the server model knowledge to improve their feature extraction capability.

Improved Alternating Minimization. After plugging Eq. (6) and (7) into our reformulation (Eq. (2) and (5)), we propose a variant of Alternating Minimization (AM) [14, 15, 16, 17, 18, 19] to solve the reformulated optimization problem as follows:

$$\underset{\mathbf{W}_s}{\operatorname{argmin}} F_s(\mathbf{W}_s, \mathbf{W}_e^{(k)*}) = \underset{\mathbf{W}_s}{\operatorname{argmin}} \sum_{k=1}^K \sum_{i=1}^{N^{(k)}} \ell_{CE}(f_s(\mathbf{W}_s; \underbrace{f_e^{(k)}(\mathbf{W}_e^{(k)*}; \mathbf{X}_i^{(k)})}_{\mathbf{H}_i^{(k)}}), y_i^{(k)}) + \sum_{k=1}^K \ell_{KD}(z_c^{(k)*}, z_s) \quad (8)$$

$$\text{where } z_c^{(k)*} = f_c^{(k)}(\mathbf{W}_c^{(k)}; \underbrace{f_e^{(k)}(\mathbf{W}_e^{(k)*}; \mathbf{X}_i^{(k)})}_{\mathbf{H}_i^{(k)}}), \text{ and } z_s = f_s(\mathbf{W}_s; \mathbf{H}_i^{(k)}) \quad (9)$$

$$\underset{\mathbf{W}^{(k)}}{\operatorname{argmin}} F_c(\mathbf{W}_s^*, \mathbf{W}^{(k)}) = \underset{\mathbf{W}^{(k)}}{\operatorname{argmin}} \sum_{i=1}^{N^{(k)}} \ell_{CE}(f_c^{(k)}(\mathbf{W}_c^{(k)}; \underbrace{f_e^{(k)}(\mathbf{W}_e^{(k)}; \mathbf{X}_i^{(k)})}_{\mathbf{H}_i^{(k)}}), y_i^{(k)}) + \ell_{KD}(z_s^*, z_c^{(k)}) \quad (10)$$

$$\text{where } z_c^{(k)} = f_c^{(k)}(\mathbf{W}_c^{(k)}; \underbrace{f_e^{(k)}(\mathbf{W}_e^{(k)}; \mathbf{X}_i^{(k)})}_{\mathbf{H}_i^{(k)}}), \text{ and } z_s^* = f_s(\mathbf{W}_s^*; \mathbf{H}_i^{(k)}) \quad (11)$$

Where the * superscript notation in above equations presents related random variable \mathbf{W} is fixed. $\mathbf{W}^{(k)}$ is the combination of $\mathbf{W}_e^{(k)}$ and $\mathbf{W}_c^{(k)}$. AM is a solver in convex and non-convex optimization theory and practice that optimize two random variables alternatively. In Eq. (8), we fix $\mathbf{W}^{(k)}$ and optimize (train) \mathbf{W}_s for epochs, and then we switch to (10) to fix \mathbf{W}_s and optimize $\mathbf{W}^{(k)}$ for epochs. This optimization persists many rounds between Eq. (8) and (10) until reaching a convergence state.

Algorithm 1 Group Knowledge Transfer. The subscript s and k stands for the server and the k th edge, respectively. E is the number of *local* epochs, T is the number of communication rounds; η is the learning rate; X represents input images; X_e is the extracted feature map; Z is the logit.

<pre> 1: Server executes: 2: for each round $t = 1, 2, \dots, T$ do 3: for each client k in parallel do 4: $X_e^k, Z_k \leftarrow \text{ClientLocalTraining}(k)$ 5: $Z_s \leftarrow$ empty dictionary 6: for each local epoch i from 1 to E_s do 7: for each client k do 8: for batch $b_idx, b \in \{X_e^k, Z_k, Y^k\}$ do 9: $w_s \leftarrow w_s - \eta_s \nabla \ell_s(b; w_s, \alpha_s)$ 10: if $i == E_s$ then 11: $Z_s[k][b_idx] \leftarrow f_s(x_e; w_s, \alpha_s)$ 12: // illustrated as "transfer back" in Fig. 1(a) 13: for each client $k \in S_t$ in parallel do 14: send the server logits $Z_s[k]$ to client k 15: </pre>	<pre> 16: ClientLocalTraining(k): // Run on client k 17: // illustrated as "local training" in Fig. 1(a) 18: for each local epoch i from 1 to E_c do 19: for batch $b \in \{X^k, Z_s[k], Y^k\}$ do 20: // $\ell_c^{(k)}$ is computed using Eq. (7) 21: $w_k \leftarrow w_k - \eta_k \nabla \ell_c^{(k)}(b; w_k, \alpha_k)$ 22: // extract features and logits 23: $X_e^k, Z_k \leftarrow$ empty dictionary 24: for batch index b_idx, batch $b \in \mathcal{B}$ do 25: $x_e^k \leftarrow f_e^k(x_i; w_e^k, \alpha_e^k)$ 26: $z_k \leftarrow f_c(f_e^k(x_i; w_e^k, \alpha_e^k), y_i; w_c, \alpha_c)$ 27: $X_e^k[b_idx] \leftarrow x_e^k$ 28: $Z_k[b_idx] \leftarrow z_k$ 29: return X_e^k, Z_k to server </pre>
-----------------------------------------------------------------------------------------------------------------------------------------------------------------------------------------------------------------------------------------------------------------------------------------------------------------------------------------------------------------------------------------------------------------------------------------------------------------------------------------------------------------------------------------------------------------------------------------------------------------------------------------------------------------------------------------------------------------------------------------------------------------------------------------------------------------------------------------------------------------------------------------------------------------------------------------------------------------------------------------------------------	---------------------------------------------------------------------------------------------------------------------------------------------------------------------------------------------------------------------------------------------------------------------------------------------------------------------------------------------------------------------------------------------------------------------------------------------------------------------------------------------------------------------------------------------------------------------------------------------------------------------------------------------------------------------------------------------------------------------------------------------------------------------------------------------------------------------------------------------------------------------------------------------------------------------------------------------------------------------------------------

Key Insight. The essence of our reformulation is that the alternating minimization (Eq. (8) and Eq. (10)) uses knowledge distillation across all edges to simplify the optimization, which scales the dataset limitation on each edge in federated learning. In particular, we achieve this objective using a local cross-entropy loss computed based only on the ground truth and the model output, and a second loss that uses the KL divergence across edges and the server, which effectively captures the contribution (knowledge) from multiple client datasets. Moreover, each minimization subproblem can be solved with SGD and its variants (e.g., SGD with momentum [50], ADAM [51, 52]).

Training Algorithm. To implement GKT as described above, we design an alternating and periodical training algorithm. To elaborate, we illustrate the entire training algorithm in Fig. 1(a) and summarize it as Algorithm 1. During each round of training, the client uses local SGD to train several epochs and then sends the extracted features and its logits to the server. When the server receives extracted features and logits from each client, it trains the much larger server-side CNN. The server then sends back its global logits to each client. This process iterates over multiple rounds, and during each round the knowledge of all clients is transferred to the server model and vice-versa. For the GKT training framework, the remaining step is designing specific neural architectures for the client model and the server model. To evaluate the effectiveness of GKT, we design CNN architectures based on ResNet [1], which are shown in Fig. 1(b). More details can also be found in Appendix B.3.

4 Experiments

4.1 Experimental Setup

A Distributed Training Library to Support GKT. Note that the popular deep learning frameworks PyTorch [53] and TensorFlow [54] cannot fully support our GKT algorithm (e.g. they only support gradient/model exchanging, while our GKT requires exchanging soft labels and hidden vectors). Thus, to simplify the usage of our GKT training framework, we use FedML [55], an open source federated learning library that simplifies the new algorithm development, and deploy it in a distributed computing environment. Our server node has 4 NVIDIA RTX 2080Ti GPUs with sufficient GPU memory for large model training. We use several CPU-based nodes as clients training small CNNs.

Task and Dataset. Our training task is image classification on CIFAR-10 [24], CIFAR-100 [24], and CINIC-10 [25]. We also generate their non-IID variants by splitting training samples into K unbalanced partitions. Details of these three datasets are introduced in Appendix A.1. The test images are used for a global test after each round. For different methods, we record the top 1 test accuracy as the metric to compare model performance. Note that we do not use FL benchmark datasets published recently (e.g., LEAF [56]) because the benchmark models provided are tiny models (CNN with only a few layers) or the datasets they contains are too easy for CNNs (e.g., MNIST), which are unable to adequately evaluate our algorithm running on large CNN models.

Baselines. We compare GKT with state-of-the-art FL method FedAvg [6], and a centralized training approach. Split Learning-based method [12, 13] is used to compare the communication cost. Note that we do not compare with FedProx [10] because it performs worse than FedAvg in the large CNN setting, as demonstrated in [8]. FedMA [8] can work on VGG [57], but it does not support batch normalization. Thus, it cannot work on ResNet.

Model Architectures. Two modern CNN architectures are evaluated: ResNet-56 and ResNet-110 [1]. The baseline FedAvg requires all edge nodes to train using these two CNNs. For GKT, the edge and server-sided models are designed based on these two CNNs. On the edge, we design a tiny CNN architecture called ResNet-8, which is a compact CNN containing 8 convolutional layers (described in Fig. 1(b) and Table 7 in Appendix). The server-sided model architectures are ResNet-55 and ResNet-109 (Table 8 and 9 in Appendix), which have the same input dimension to match the output of the edge-sided feature extractor. For split learning, we use the extractor in ResNet-8 as the edge-sided partition of CNNs, while the server-side partitions of CNN is also ResNet-55 and ResNet-109.

4.2 Result of Model Accuracy

For standard experiments, we run on 16 clients and a GPU server for all datasets and models. Fig. 3 shows the curve of the test accuracy during training on ResNet-56 model with 3 datasets. It includes the result of centralized training, FedAvg, and GKT. We also summarize all numerical results of

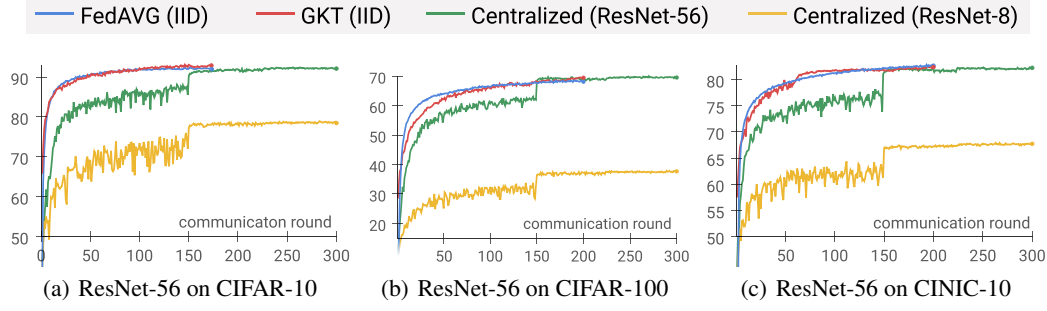


Figure 3: The Test Accuracy of ResNet-56 (Edge Number = 16)

ResNet-56 and ResNet-110 in Table 1. In both IID and non-IID setting, GKT obtains comparable or even better accuracy than FedAvg.

Hyperparameters. There are four important hyper-parameters in our GKT framework: the communication round, as stated in line #2 of Algorithm 1, the edge-side epoch number, the server-side epoch number, and the server-side learning rate. After a tuning effort, we find that the edge-side epoch number can be just 1. The server epoch number depends on the data distribution. For IID data, it is 20, and for non-IID, the value depends on the level of data bias. For IID, Adam optimizer [51] works better than SGD with momentum [50], while for non-IID, SGD with momentum works better. During training, we reduce the learning rate once the accuracy has plateaued [58, 59]. We use the same data augmentation techniques for fair comparison (random crop, random horizontal flip, and normalization). More details of hyper-parameters are described in Appendix B.4.

Table 1: The Test Accuracy of ResNet-56 and ResNet-110 on Three Datasets.

Model	Methods	CIFAR-10		CIFAR-100		CINIC-10	
		IID	non-IID	IID	non-IID	IID	non-IID
ResNet-56	GKT (ResNet-8, ours)	92.97	86.59	69.57	63.76	81.51	77.80
	FedAvg (ResNet-56)	92.88	86.60	68.09	63.78	81.62	77.85
	Centralized (ResNet-56)		93.05		69.73		81.66
	Centralized (ResNet-8)		78.94		37.67		67.72
ResNet-110	GKT (ResNet-8, ours)	93.47	87.18	69.87	64.31	81.98	78.39
	FedAvg (ResNet-56)	93.49	87.20	68.58	64.35	82.10	78.43
	Centralized (ResNet-56)		93.58		70.18		82.16
	Centralized (ResNet-8)		78.94		37.67		67.72

*Note: 1. It is a normal phenomenon when the test accuracy in non-IID is lower than that of IID. This is confirmed by both this study and other CNN-based FL works [26, 27]; 2. In the non-IID setting, since the model performance is sensitive to the data distribution, we fix the distribution of non-IID dataset for a fair comparison. Appendix A.2 describes the specific non-IID distribution used in the experiment; 3. Table 10, 11, 12 in Appendix summarize the corresponding hyperparameters used in the experiments.

4.3 Efficiency Evaluation

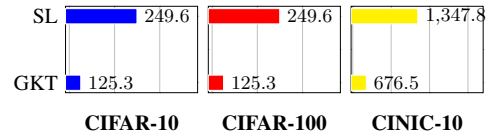
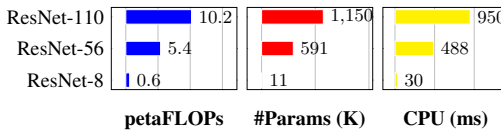


Figure 4: Edge Computational Efficiency (CIFAR-100)

Figure 5: Communication Efficiency (ResNet-56)

To compare the computational demand on training, we count the number of FLOPs (floating-point operations) performed on edge using prior methods [60, 61]. We report the result on CIFAR-100 in Fig. 4. Compared to the FedAvg baseline, the computational cost on the edge of our GKT (ResNet-8) is 9 times less than that of ResNet-56 and 17 times less than that of ResNet-110 (The memory cost comparison can be roughly compared by the model parameter number: ResNet-8 has 11K parameters, which is 54 times less than that of ResNet-56 and 105 times less than that of ResNet-110. We also

test the CPU running time per mini-batch (batch size is 64) forward-backward propagation on Intel i7 CPU (which has a more aggressive performance than current edge devices). The results show that ResNet-8 requires only 3% of ResNet-110’s training time (30 ms v.s. 950 ms).

To compare communication costs, we use SL [12, 13] as the baseline, which also exchanges hidden feature maps rather than the entire model. The communication cost is calculated using Eq. (12) and (13) in Appendix B.2 without using data compression techniques. The results are shown in Fig. 5 (X-axis units: GBytes). GKT uses fewer feature map exchanges with the server than SL.

4.4 Ablation Study: Understanding GKT under Different Settings

Table 2: Ablation Study on Loss Functions

	CIFAR-10	CIFAR-100	CINIC-10
None	diverge	diverge	diverge
Only S->E	92.97	68.44	81.51
Both	90.53	69.57	80.01

Table 3: Asynchronous Training

	CIFAR-10	CIFAR-100	CINIC-10
Sync	92.97	69.57	81.51
Async	92.92	69.65	81.43

The Effectiveness of Bi-directional Knowledge Transfer. In this study we evaluate the efficacy of using knowledge distillation loss, ℓ_{KD} in Eq. (7) and Eq. (6). Table 2 shows the results. We created one scenario labeled *None* in the table where both the client and server only use ℓ_{CE} and do not use ℓ_{KD} . In another scenario, only the clients use ℓ_{CE} to update their local models, but the server does not (*only S->E*). If we do not use knowledge transfer at all, the training will diverge (as shown for *None*). Moreover, the transfer from the server to the edge always helps (*only S->E*), while the transfer from the edge to the server is more helpful as the dataset becomes increasingly difficult (CIFAR-100).

Asynchronous Training. Since the server does not need to wait for updates from all clients to start training, GKT naturally supports asynchronous training. We present the experimental results in Table 3. It proves that asynchronous training does not negatively affect model accuracy. This demonstrates the advantage of our method over SL, in which every edge requires multiple synchronizations for each mini-batch iteration.

Table 4: GKT with Different Edge Number

	8	16	64	128
GKT	69.51	69.57	69.65	69.59

Table 5: Small CNNs on CIFAR-10

	ResNet-4	ResNet-6	ResNet-8
Test Accuracy	88.86	90.32	92.97

GKT with Different Edge Number. To understand the scalability of GKT, we evaluate its performance with varying edge nodes. The test accuracy results are shown in Table 4. In general, adding more edge nodes does not negatively affect accuracy.

Smaller Architectures. We test the performance of GKT using even smaller edge models: ResNet-4, ResNet-6 on CIFAR-10. ResNet-4 and ResNet-6 use one and two BasicBlock components (including two convolutional layers), respectively. The result is shown in Table 5. While reducing the edge model size to ResNet-8 did not reduce accuracy, when the model size is reduced even more substantially, it does reduce the overall accuracy.

5 Conclusion

In this work, to tackle the resource-constrained reality, we reformulate FL as a group knowledge transfer (GKT) training algorithm. GKT can efficiently train small CNNs on edges and periodically transfer their knowledge by knowledge distillation to a server-side CNN with a large capacity. GKT achieves several advantages in a single framework: reduced demand for edge computation, lower communication cost for large CNNs, and asynchronous training, all while maintaining model accuracy comparable to FL. To simplify the edge training, we also develop a distributed training system based on our GKT. We evaluate GKT by training modern CNN architectures (ResNet-56 and ResNet-110) on three distinct datasets (CIFAR-10, CIFAR-100, and CINIC-10) and their non-IID variants. Our results show that GKT can obtain comparable or even slightly higher accuracy. More importantly, GKT makes edge training affordable. Compared to the edge training using FedAvg, GKT costs 9 to 17 times less computational power (FLOPs) and requires 54 to 105 times fewer parameters.

Broader Impact

GKT can efficiently train large deep neural networks (CNNs) in resource-constrained edge devices (such as smartphones, IoT devices, and edge servers). Unlike past FL approaches, GKT demonstrates the feasibility of training a large server-side model by using many small client models. GKT preserves the data privacy requirements of the FL approach but also works within the constraints of an edge computing environment. Smartphone users may benefit from this technique because their private data is protected, and they may also simultaneously obtain a high-quality model service. Organizations such as hospitals, and other non-profit entities with limited training resources, can collaboratively train a large CNN model without revealing their datasets while achieving significant training cost savings. They can also meet the requirements regarding the protection of intellectual property, confidentiality, regulatory restrictions, and legal constraints.

As for the potential risks of our method, a client can maliciously send incorrect hidden feature maps and soft labels to the server, which may potentially impact the overall model accuracy. These effects must be detected and addressed to maintain overall system stability. Second, the relative benefits for each client may vary. For instance, in terms of fairness, edge nodes which have smaller datasets may obtain more model accuracy improvement from collaborative training than those which have a larger amount of training data. Our training framework does not consider how to balance this interest of different parties.

References

- [1] He, K., X. Zhang, S. Ren, et al. Deep residual learning for image recognition. In *Proceedings of the IEEE conference on computer vision and pattern recognition*, pages 770–778. 2016.
- [2] Liu, H., K. Simonyan, Y. Yang. Darts: Differentiable architecture search. *arXiv preprint arXiv:1806.09055*, 2018.
- [3] He, C., H. Ye, L. Shen, et al. Milenas: Efficient neural architecture search via mixed-level reformulation. *arXiv preprint arXiv:2003.12238*, 2020.
- [4] Tan, M., Q. V. Le. Efficientnet: Rethinking model scaling for convolutional neural networks. *arXiv preprint arXiv:1905.11946*, 2019.
- [5] Kairouz, P., H. B. McMahan, B. Avent, et al. Advances and open problems in federated learning. *arXiv preprint arXiv:1912.04977*, 2019.
- [6] McMahan, H. B., E. Moore, D. Ramage, et al. Communication-efficient learning of deep networks from decentralized data. *arXiv preprint arXiv:1602.05629*, 2016.
- [7] He, C., C. Tan, H. Tang, et al. Central server free federated learning over single-sided trust social networks. *arXiv preprint arXiv:1910.04956*, 2019.
- [8] Wang, H., M. Yurochkin, Y. Sun, et al. Federated learning with matched averaging. *arXiv preprint arXiv:2002.06440*, 2020.
- [9] Bonawitz, K., H. Eichner, W. Grieskamp, et al. Towards federated learning at scale: System design. *arXiv preprint arXiv:1902.01046*, 2019.
- [10] Li, T., A. K. Sahu, M. Zaheer, et al. Federated optimization in heterogeneous networks. *arXiv preprint arXiv:1812.06127*, 2018.
- [11] Yu, H., S. Yang, S. Zhu. Parallel restarted sgd with faster convergence and less communication: Demystifying why model averaging works for deep learning. In *Proceedings of the AAAI Conference on Artificial Intelligence*, vol. 33, pages 5693–5700. 2019.
- [12] Gupta, O., R. Raskar. Distributed learning of deep neural network over multiple agents. *Journal of Network and Computer Applications*, 116:1–8, 2018.
- [13] Vepakomma, P., O. Gupta, T. Swedish, et al. Split learning for health: Distributed deep learning without sharing raw patient data. *arXiv preprint arXiv:1812.00564*, 2018.
- [14] Ortega, J. M., W. C. Rheinboldt. *Iterative solution of nonlinear equations in several variables*, vol. 30. Siam, 1970.

- [15] Bertsekas, D. P., J. N. Tsitsiklis. *Parallel and distributed computation: numerical methods*, vol. 23. Prentice hall Englewood Cliffs, NJ, 1989.
- [16] Bolte, J., S. Sabach, M. Teboulle. Proximal alternating linearized minimization for nonconvex and nonsmooth problems. *Mathematical Programming*, 146(1-2):459–494, 2014.
- [17] Attouch, H., J. Bolte, P. Redont, et al. Proximal alternating minimization and projection methods for nonconvex problems: An approach based on the kurdyka-lojasiewicz inequality. *Mathematics of Operations Research*, 35(2):438–457, 2010.
- [18] Wright, S. J. Coordinate descent algorithms. *Mathematical Programming*, 151(1):3–34, 2015.
- [19] Razaviyayn, M., M. Hong, Z.-Q. Luo. A unified convergence analysis of block successive minimization methods for nonsmooth optimization. *SIAM Journal on Optimization*, 23(2):1126–1153, 2013.
- [20] Hinton, G., O. Vinyals, J. Dean. Distilling the knowledge in a neural network. *arXiv preprint arXiv:1503.02531*, 2015.
- [21] Buciluă, C., R. Caruana, A. Niculescu-Mizil. Model compression. In *Proceedings of the 12th ACM SIGKDD international conference on Knowledge discovery and data mining*, pages 535–541. 2006.
- [22] Ba, J., R. Caruana. Do deep nets really need to be deep? In *Advances in neural information processing systems*, pages 2654–2662. 2014.
- [23] Romero, A., N. Ballas, S. E. Kahou, et al. Fitnets: Hints for thin deep nets. *arXiv preprint arXiv:1412.6550*, 2014.
- [24] Krizhevsky, A., G. Hinton, et al. Learning multiple layers of features from tiny images. 2009.
- [25] Darlow, L. N., E. J. Crowley, A. Antoniou, et al. Cinic-10 is not imagenet or cifar-10. *arXiv preprint arXiv:1810.03505*, 2018.
- [26] Hsieh, K., A. Phanishayee, O. Mutlu, et al. The non-iid data quagmire of decentralized machine learning. *arXiv preprint arXiv:1910.00189*, 2019.
- [27] Reddi, S., Z. Charles, M. Zaheer, et al. Adaptive federated optimization. *arXiv preprint arXiv:2003.00295*, 2020.
- [28] Bernstein, J., Y.-X. Wang, K. Azizzadenesheli, et al. signsgd: Compressed optimisation for non-convex problems. *arXiv preprint arXiv:1802.04434*, 2018.
- [29] Wangni, J., J. Wang, J. Liu, et al. Gradient sparsification for communication-efficient distributed optimization. In *Advances in Neural Information Processing Systems*, pages 1299–1309. 2018.
- [30] Tang, H., S. Gan, C. Zhang, et al. Communication compression for decentralized training. In *Advances in Neural Information Processing Systems*, pages 7652–7662. 2018.
- [31] Alistarh, D., D. Grubic, J. Li, et al. Qsgd: Communication-efficient sgd via gradient quantization and encoding. In *Advances in Neural Information Processing Systems*, pages 1709–1720. 2017.
- [32] Lin, Y., S. Han, H. Mao, et al. Deep gradient compression: Reducing the communication bandwidth for distributed training. *arXiv preprint arXiv:1712.01887*, 2017.
- [33] Wang, H., S. Sievert, S. Liu, et al. Atomo: Communication-efficient learning via atomic sparsification. In *Advances in Neural Information Processing Systems*, pages 9850–9861. 2018.
- [34] Zhang, Y., T. Xiang, T. M. Hospedales, et al. Deep mutual learning. In *Proceedings of the IEEE Conference on Computer Vision and Pattern Recognition*, pages 4320–4328. 2018.
- [35] Anil, R., G. Pereyra, A. Passos, et al. Large scale distributed neural network training through online distillation. *arXiv preprint arXiv:1804.03235*, 2018.
- [36] Song, G., W. Chai. Collaborative learning for deep neural networks. In *Advances in Neural Information Processing Systems*, pages 1832–1841. 2018.
- [37] Jeong, E., S. Oh, H. Kim, et al. Communication-efficient on-device machine learning: Federated distillation and augmentation under non-iid private data. *arXiv preprint arXiv:1811.11479*, 2018.
- [38] Chen, D., J.-P. Mei, C. Wang, et al. Online knowledge distillation with diverse peers. *arXiv preprint arXiv:1912.00350*, 2019.

- [39] Park, J., S. Wang, A. Elgabli, et al. Distilling on-device intelligence at the network edge. *arXiv preprint arXiv:1908.05895*, 2019.
- [40] Tran, L., B. S. Veeling, K. Roth, et al. Hydra: Preserving ensemble diversity for model distillation. *arXiv preprint arXiv:2001.04694*, 2020.
- [41] Zhu, X., S. Gong, et al. Knowledge distillation by on-the-fly native ensemble. In *Advances in neural information processing systems*, pages 7517–7527. 2018.
- [42] Vongkulbhisal, J., P. Vinayavekhin, M. Visentini-Scarzanella. Unifying heterogeneous classifiers with distillation. In *Proceedings of the IEEE Conference on Computer Vision and Pattern Recognition*, pages 3175–3184. 2019.
- [43] Han, S., H. Mao, W. J. Dally. Deep compression: Compressing deep neural networks with pruning, trained quantization and huffman coding. *arXiv preprint arXiv:1510.00149*, 2015.
- [44] He, Y., J. Lin, Z. Liu, et al. Amc: Automl for model compression and acceleration on mobile devices. In *Proceedings of the European Conference on Computer Vision (ECCV)*, pages 784–800. 2018.
- [45] Yang, T.-J., A. Howard, B. Chen, et al. Netadapt: Platform-aware neural network adaptation for mobile applications. In *Proceedings of the European Conference on Computer Vision (ECCV)*, pages 285–300. 2018.
- [46] Howard, A. G., M. Zhu, B. Chen, et al. Mobilenets: Efficient convolutional neural networks for mobile vision applications. *arXiv preprint arXiv:1704.04861*, 2017.
- [47] Zhang, X., X. Zhou, M. Lin, et al. Shufflenet: An extremely efficient convolutional neural network for mobile devices. In *Proceedings of the IEEE conference on computer vision and pattern recognition*, pages 6848–6856. 2018.
- [48] Iandola, F. N., S. Han, M. W. Moskewicz, et al. Squeezenet: Alexnet-level accuracy with 50x fewer parameters and < 0.5 mb model size. *arXiv preprint arXiv:1602.07360*, 2016.
- [49] Wu, B., X. Dai, P. Zhang, et al. Fbnet: Hardware-aware efficient convnet design via differentiable neural architecture search. In *Proceedings of the IEEE Conference on Computer Vision and Pattern Recognition*, pages 10734–10742. 2019.
- [50] Qian, N. On the momentum term in gradient descent learning algorithms. *Neural networks*, 12(1):145–151, 1999.
- [51] Kingma, D. P., J. Ba. Adam: A method for stochastic optimization. *arXiv preprint arXiv:1412.6980*, 2014.
- [52] Zou, F., L. Shen, Z. Jie, et al. A sufficient condition for convergences of adam and rmsprop. In *Proceedings of the IEEE Conference on Computer Vision and Pattern Recognition*, pages 11127–11135. 2019.
- [53] Paszke, A., S. Gross, F. Massa, et al. Pytorch: An imperative style, high-performance deep learning library. In *Advances in Neural Information Processing Systems*, pages 8024–8035. 2019.
- [54] Abadi, M., P. Barham, J. Chen, et al. Tensorflow: A system for large-scale machine learning. In *12th {USENIX} Symposium on Operating Systems Design and Implementation ({OSDI} 16)*, pages 265–283. 2016.
- [55] He, C., S. Li, J. So, et al. Fedml: A research library and benchmark for federated machine learning. *arXiv preprint arXiv:2007.13518*, 2020.
- [56] Caldas, S., P. Wu, T. Li, et al. Leaf: A benchmark for federated settings. *arXiv preprint arXiv:1812.01097*, 2018.
- [57] Simonyan, K., A. Zisserman. Very deep convolutional networks for large-scale image recognition. *arXiv preprint arXiv:1409.1556*, 2014.
- [58] Li, Z., S. Arora. An exponential learning rate schedule for deep learning. *arXiv preprint arXiv:1910.07454*, 2019.
- [59] Shi, B., W. J. Su, M. I. Jordan. On learning rates and schrödinger operators. *arXiv preprint arXiv:2004.06977*, 2020.
- [60] OpenAI. Ai and compute, 2018. <https://openai.com/blog/ai-and-compute>.
- [61] Hernandez, D., T. B. Brown. Measuring the algorithmic efficiency of neural networks. *arXiv preprint arXiv:2005.04305*, 2020.

A Datasets

A.1 A Summary of Dataset Used in Experiments

CIFAR-10 [24] consists of 60000 32×32 colour images in 10 classes, with 6000 images per class. There are 50000 training images and 10000 test images. **CIFAR-100** [24] has the same amount of samples as CIFAR-10, but it is a more challenging dataset since it has 100 classes containing 600 images each. **CINIC-10** [25] has a total of 270,000 images, 4.5 times that of CIFAR-10. It is constructed from two different sources: ImageNet and CIFAR-10. It is not a guaranteed that the constituent elements are drawn from the same distribution. This characteristic fits for federated learning because we can evaluate how well models cope with samples drawn from similar but not identical distributions. CINIC-10 has three sub-datasets: training, validation, and testing. We train on the training dataset and test on the testing, without using the validation dataset for all experiments. Our source code provides link to download these three datasets.

For the non-IID dataset, the partition is unbalanced: sampling $\mathbf{p}_c \sim \text{Dir}_J(0.5)$ and allocating a $\mathbf{p}_{c,k}$ proportion of the training samples of class c to local client k .

A.2 Heterogeneous Distribution (non-IID) in Each Client

We fix the non-IID distribution to fairly compare different methods. Table 6 is a specific distribution used in experiments. We also conduct experiments in other non-IID distributions and see that our GKT method also beats baselines. To generate the different distribution, we can change the random seed in *main.py* of our source code.

Client ID	Numbers of Samples in the Classes										Distribution
	c_0	c_1	c_2	c_3	c_4	c_5	c_6	c_7	c_8	c_9	
k=0	144	94	1561	133	1099	1466	0	0	0	0	
k=1	327	28	264	16	354	2	100	20	200	3	
k=2	6	6	641	1	255	4	1	2	106	1723	
k=3	176	792	100	28	76	508	991	416	215	0	
k=4	84	1926	1	408	133	24	771	0	0	0	
k=5	41	46	377	541	7	235	54	1687	666	0	
k=6	134	181	505	720	123	210	44	58	663	221	
k=7	87	2	131	1325	1117	704	0	0	0	0	
k=8	178	101	5	32	1553	10	163	9	437	131	
k=9	94	125	0	147	287	100	23	217	608	279	
k=10	379	649	106	90	35	119	807	819	3	85	
k=11	1306	55	681	227	202	34	0	648	0	0	
k=12	1045	13	53	6	77	70	482	7	761	494	
k=13	731	883	15	161	387	552	4	1051	0	0	
k=14	4	97	467	899	0	407	50	64	1098	797	
k=15	264	2	93	266	412	142	806	2	243	1267	

Table 6: The actual heterogeneous data distribution (non-IID) generated from CIFAR-10

B Extra Experimental Results and Details

B.1 Computational Efficiency on CIFAR-10 and CINIC-10

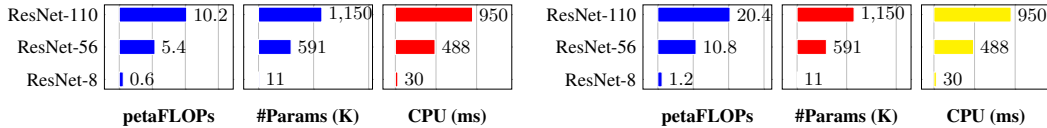


Figure 6: Edge Computational Efficiency (CIFAR-100) Figure 7: Edge Computational Efficiency (CINIC-10)

B.2 The Method of Communication Cost Calculation

For split learning (SL), the method to calculate the communication cost is:

$$\begin{aligned} \text{Communication Cost of SL} = & (\text{the size of the hidden feature map} + \text{the size of the gradient in the split layer}) \\ & \times (\text{number of samples in dataset}) \times (\text{number of epochs}) \end{aligned} \quad (12)$$

For GKT, the method to calculate the communication cost is:

$$\begin{aligned} \text{Communication Cost of GKT} = & (\text{the size of the hidden feature map} + \\ & \text{the size of soft labels received from the server side}) \times (\text{number of samples in dataset}) \\ & \times (\text{number of communication rounds}) \end{aligned} \quad (13)$$

B.3 Details of Convolutional Neural Architecture on Edge and Server

ResNet-8 is a compact CNN. Its head convolutional layer (including batch normalization and ReLU non-linear activation) is used as the feature extractor. The remaining two Bottlenecks (a classical component in ResNet, each containing 3 convolutional layers) and the last fully-connected layer are used as the classifier.

Table 7: Detailed information of the ResNet-8 architecture used in our experiment

Layer	Parameter & Shape (cin, cout, kernal size) & hyper-parameters	#
layer1	conv1: $3 \times 16 \times 3 \times 3$, stride:(1, 1); padding:(1, 1)	$\times 1$
	maxpool: 3×1	$\times 1$
	conv1: $16 \times 16 \times 3 \times 3$, stride:(1, 1); padding:(1, 1)	$\times 3$
	conv2: $16 \times 16 \times 3 \times 3$, stride:(1, 1); padding:(1, 1)	
	avgpool	$\times 1$
	fc: 16×10	$\times 1$

Table 8: Detailed information of the ResNet-55 architecture used in our experiment

Layer	Parameter & Shape (cin, cout, kernal size) & hyper-parameters	#
layer1	conv1: $16 \times 16 \times 1 \times 1$, stride:(1, 1)	$\times 1$
	conv2: $16 \times 16 \times 3 \times 3$, stride:(1, 1); padding:(1, 1)	
	conv3: $16 \times 64 \times 1 \times 1$, stride:(1, 1)	
	downsample.conv: $16 \times 64 \times 1 \times 1$, stride:(1, 1)	
	conv1: $64 \times 16 \times 1 \times 1$, stride:(1,1)	$\times 5$
layer2	conv2: $16 \times 16 \times 3 \times 3$, stride:(1, 1), padding:(1,1)	
	conv3: $16 \times 64 \times 1 \times 1$, stride:(1, 1)	
	conv1: $64 \times 32 \times 1 \times 1$, stride:(1, 1)	$\times 1$
	conv2: $32 \times 32 \times 3 \times 3$, stride:(2, 2); padding:(1, 1)	
	conv3: $32 \times 128 \times 1 \times 1$, stride:(1, 1)	
	downsample.conv: $64 \times 128 \times 1 \times 1$, stride:(2, 2)	
layer3	conv1: $128 \times 32 \times 1 \times 1$, stride:(1, 1)]	$\times 5$
	conv2: $32 \times 32 \times 3 \times 3$, stride:(1, 1); padding:(1, 1)	
	conv3: $32 \times 128 \times 1 \times 1$, stride:(1, 1)	
	conv1: $128 \times 64 \times 1 \times 1$, stride:(1, 1)	$\times 1$
	conv2: $64 \times 64 \times 3 \times 3$, stride:(2, 2); padding:(1, 1)	
	conv3: $64 \times 256 \times 1 \times 1$, stride:(1, 1)	
	downsample.conv: $128 \times 256 \times 1 \times 1$, stride:(2, 2)	
	conv1: $256 \times 64 \times 1 \times 1$, stride:(1, 1)	$\times 5$
	conv2: $64 \times 64 \times 3 \times 3$, stride:(1, 1); padding:(1, 1)	
	conv3: $64 \times 256 \times 1 \times 1$, stride:(1, 1)	
	avgpool	$\times 1$
	fc: 256×10	$\times 1$

B.4 Hyperparameters

In table 10, 11, and 12, we summarize the hyperparameter settings for all experiments. If applying our GKT framework to a new CNN architecture with different datasets, we suggest tuning all hyper-parameters based on our hyperparameters.

Table 9: Detailed information of the ResNet-109 architecture used in our experiment

Layer	Parameter & Shape (cin, cout, kernal size) & hyper-parameters	#
layer1	conv1: $16 \times 16 \times 1 \times 1$, stride:(1, 1)	$\times 1$
	conv2: $16 \times 16 \times 3 \times 3$, stride:(1, 1); padding:(1, 1)	
	conv3: $16 \times 64 \times 1 \times 1$, stride:(1, 1)	
	downsample.conv: $16 \times 64 \times 1 \times 1$, stride:(1, 1)	
layer2	conv1: $64 \times 16 \times 1 \times 1$, stride:(1,1)	$\times 11$
	conv2: $16 \times 16 \times 3 \times 3$, stride:(1, 1), padding:(1,1)	
	conv3: $16 \times 64 \times 1 \times 1$, stride:(1, 1)	
layer3	conv1: $64 \times 32 \times 1 \times 1$, stride:(1, 1)	$\times 1$
	conv2: $32 \times 32 \times 3 \times 3$, stride:(2, 2); padding:(1, 1)	
	conv3: $32 \times 128 \times 1 \times 1$, stride:(1, 1)	
	downsample.conv: $64 \times 128 \times 1 \times 1$, stride:(2, 2)	
layer4	conv1: $128 \times 32 \times 1 \times 1$, stride:(1, 1)]	$\times 11$
	conv2: $32 \times 32 \times 3 \times 3$, stride:(1, 1); padding:(1, 1)	
	conv3: $32 \times 128 \times 1 \times 1$, stride:(1, 1)	
layer5	conv1: $128 \times 64 \times 1 \times 1$, stride:(1, 1)	$\times 1$
	conv2: $64 \times 64 \times 3 \times 3$, stride:(2, 2); padding:(1, 1)	
	conv3: $64 \times 256 \times 1 \times 1$, stride:(1, 1)	
	downsample.conv: $128 \times 256 \times 1 \times 1$, stride:(2, 2)	
layer6	conv1: $256 \times 64 \times 1 \times 1$, stride:(1, 1)	$\times 11$
	conv2: $64 \times 64 \times 3 \times 3$, stride:(1, 1); padding:(1, 1)	
	conv3: $64 \times 256 \times 1 \times 1$, stride:(1, 1)	
avgpool		$\times 1$
fc: 256×10		$\times 1$

Table 10: Hyperparameters used in Experiments on dataset CIFAR-10

Model	Methods	Hyperparameters	CIFAR-10	
			IID	non-IID
ResNet-56/110	GKT (ours)	optimizer	Adam, lr=0.001, wd=0.0001	SGD, lr=0.005, momentum=0.9
		batch size	256	256
		edge epochs	1	1
		server epochs	20	40
		communication rounds	200	200
	FedAvg	optimizer	Adam, lr=0.001, wd=0.0001	Adam, lr=0.001, wd=0.0001
		batch size	64	64
		local epochs	20	20
		communication rounds	200	200
	Centralized	optimizer	Adam, lr=0.003, wd=0.0001	
		batch size	256	
		epochs	300	
	Centralized (ResNet-8)	optimizer	Adam, lr=0.003, wd=0.0001	
		batch size	256	
		epochs	300	

Table 11: Hyperparameters used in Experiments on dataset CIFAR-100

Model	Methods	Hyperparameters	CIFAR-100	
			IID	non-IID
ResNet-56/110	GKT (ours)	optimizer	Adam, lr=0.001, wd=0.0001	SGD, lr=0.005, momentum=0.9
		batch size	256	256
		edge epochs	1	1
		server epochs	20	40
		communication rounds	200	200
	FedAvg	optimizer	Adam, lr=0.001, wd=0.0001	Adam, lr=0.001, wd=0.0001
		batch size	64	64
		local epochs	20	20
		communication rounds	200	200
	Centralized	optimizer	Adam, lr=0.003, wd=0.0001	
		batch size	256	
		epochs	300	
	Centralized (ResNet-8)	optimizer	Adam, lr=0.003, wd=0.0001	
		batch size	256	
		epochs	300	

Table 12: Hyperparameters used in Experiments on dataset CINIC-10

Model	Methods	Hyperparameters	CINIC-10	
			IID	non-IID
ResNet-56/110	GKT (ours)	optimizer	Adam, lr=0.001, wd=0.0001	SGD, lr=0.005, momentum=0.9
		batch size	256	256
		edge epochs	1	1
		server epochs	20	40
		communication rounds	200	200
	FedAvg	optimizer	Adam, lr=0.001, wd=0.0001	Adam, lr=0.001, wd=0.0001
		batch size	64	64
		local epochs	20	20
		communication rounds	200	200
	Centralized	optimizer	Adam, lr=0.003, wd=0.0001	
		batch size	256	
		epochs	300	
	Centralized (ResNet-8)	optimizer	Adam, lr=0.003, wd=0.0001	
		batch size	256	
		epochs	300	